Fully Developed Multilayer Polymer Flows in Slits and Annuli

M. E. NORDBERG III and H. H. WINTER

Goessmann Laboratory
Department of Chemical Engineering
University of Massachusetts
Amherst, Massachusetts 01003

A numerical method has been developed for simulating fully developed multilayer shear flows of non-Newtonian fluids with arbitrary viscosity functions. Poiseuille and combined Poiseuille/Couette flows in both slits and annuli may be modeled. The method employs a finite difference system where grid points lie on streamlines and move to their correct positions as the solution procedure converges. Interfaces are easily handled as particular streamlines with the equation of motion replaced by a boundary condition. The method is stable for high interface viscosity ratios and readily handles a large number of layers. Many authors have employed power law models to model multilayer non-Newtonian flows. We find that the power law is sufficient to predict pressure gradients and interface positions in most cases, but gives unrealistically flat velocity profiles, even when truncated at finite viscosity. Results are presented for the Carreau fluid and for the rubber-like liquid with shear thinning via Wagner's strain functional.

INTRODUCTION

Many of the most promising new polymer processes in the packaging and container businesses make use of coextrusion blow molding or film blowing. Polymer parts, wire coatings, fibers, and sheets are also increasingly often extruded from more than one material. All of these in the fully developed case are pressure driven (Poiseuille) flows. In wire coating the moving inner wall superimposes a Couette flow.

A corresponding increase in basic fluid mechanics research has accompanied the industrial growth. The fundamental industrial problem is to design coextrusion dies and processing conditions for the efficient production of high quality parts or films. Corresponding research problems include the fully developed kinematics of planar and annular flows (1–3), evolving planar and annular kinematics (4), nonisothermal effects (5, 6), material layer rearrangements (7, 8), interface instabilities (9), multilayer die swell (10), and the multilayer distribution problem (11).

This paper considers the very basic kinematics of fully developed non-Newtonian planar or annular multilayer flows. In nearly all studies of this problem (including all those cited above) researchers have employed either a Newtonian or a power law stress constitutive equation for each fluid layer. This, in most cases, allows the analysis to be semi-analytical in nature. The present study develops a fully numerical method which allows the determination of kinematics for arbitrary non-Newtonian fluids.

BACKGROUND

The generic problem to be solved takes one of two forms. 1) Given an M-layer flow with the flow rate and material parameters of each layer specified, what are the pressure gradient and velocity profile of the flow? 2) In an M-layer flow with the total flow rate, material parameters, and interface positions given, what are the pressure gradient, velocity profile, and individual flow rates? The first of these questions is what a die designer might ask; an answer to the second is what an experimentalist might use to analyze (or predict) his or her results (12). The first problem is the one solved in this paper. However, one can solve the first by iteratively solving the second, varying the specified interface positions until desired layer flow rates are reached. The iterative solution method which we will present reduces the problem at each

step to the second question, where interface positions are given.

Two different solution approaches are well known for the solution of the two problems. Each is semi-analytical and requires an iterative procedure with two parameters specified and respecified until a converged solution is achieved. If the pressure gradient, the interface positions, and the position of zero shear are all known then the velocity profile may be found analytically for each layer by integrating the equation of motion. The velocity profile may then be integrated for total and individual flow rates.

To solve the second problem, iteratively improve guesses for the pressure gradient and zero-shear position until the total flow rate matches the desired value. See Han's book for a clear summary of this procedure in various geometries (13).

To solve the first problem, integrate the equation of motion stepwise from the inner wall, fixing an interface and switching fluids whenever the flow rate reaches the known flow for each layer. Again the pressure gradient and zero shear plane must be iteratively specified. This procedure converges when the integration over the outer layer ends exactly at the outer wall. This method is summarized by Schrenk and Alfrey (1).

Both of the above methods are essentially shooting methods. The first problem's solution involves a traditional shooting to an opposite boundary and has the traditional disadvantages of shooting methods: difficult convergence (especially with two free parameters) and potentially high sensitivity to the boundary conditions or to round-off errors, see e.g. (14). The second method has the advantage of shooting for an integral of the solution, which may be less sensitive to the choice of parameters. However, the real disadvantage of both methods is that they are applicable only for fluids whose constitutive equations allow analytical integration of the equation of motion. The methods could be extended for numerical integration of the equation of motion, but then they would suffer even more from the problems of shooting methods.

The multilayer problem can be solved numerically by modifying standard finite difference (6) or finite element (15) methods to account for the separate fluids. However, a numerical method has developed in recent years for the simulation of free surface flows: the streamlined finite element method (16–18). The interface between two coextruding fluids is a free stream surface, so a streamlined grid method is a natural candidate for simulating coextrusion flows. Streamlined finite element methods have the advantage of finding free surfaces naturally, as a matter of course, during the solution. They have the disadvantage of requiring extra overhead to move grid points at each successive iteration. If the grid points can be moved efficiently then the advantage outweighs the disadvantage.

The authors have chosen a streamlined finite difference method. Since the problem is one dimensional (i.e. variables vary over only one space dimension) an equivalent streamlined finite element method could have been derived. The authors admit to a bias towards the finite difference presentation, but the present method also generalizes to two dimensional flows where the method is truly finite difference (4).

BASIC EQUATIONS AND NUMERICAL APPROXIMATIONS

This section derives streamlined finite difference formulas for fully developed planar flow. The *Appendix* presents the corresponding derivation for axisymmetric flow.

For fully developed shear flow in a slit with constant cross-section the equation of motion and the shear stress are

$$\frac{d\tau_{xy}}{dy} = \frac{dp}{dx}, \quad \text{and} \tag{1}$$

$$\tau_{xy} = \eta(\dot{\gamma})\frac{dv}{dy}. \tag{2}$$

Equations 1 and *2* may be combined into

$$\frac{d}{dy}\left(\eta(\dot{\gamma})\frac{dv}{dy}\right) = \frac{dp}{dx}, \quad \text{or} \tag{3}$$

$$\eta(\dot{\gamma})\frac{d^2v}{dy^2} + \frac{d\eta(\dot{\gamma})}{dy}\frac{dv}{dy} = \frac{dp}{dx} \tag{4}$$

The derivation below makes no assumptions about the shear rate dependence of the steady shear viscosity, $\eta(\dot{\gamma})$, but three specific constitutive equations are used in this study, the truncated power law model (*Eq 5*), the Carreau model (*Eq 6*), and the Wagner modification of the rubber-like liquid, simplified for constant shear (19) (*Eq 7*).

$$\eta(\dot{\gamma}) = min\left(\eta_0, \eta^0\left|\frac{\dot{\gamma}}{\dot{\gamma}^0}\right|^{n-1}\right). \tag{5}$$

$$\eta(\dot{\gamma}) = \eta_\infty + (\eta_0 - \eta_\infty)[1 + (\lambda\dot{\gamma})^2]^{(n-1)/2}. \tag{6}$$

$$\eta(\dot{\gamma}) = \sum_{i=1}^{m}\sum_{j=1}^{2}\frac{f_j\lambda_i g_i}{(1 + n_j\lambda_i|\dot{\gamma}|)^2}. \tag{7}$$

All material parameters in the above equations are determined by fitting experimental data.

The solution method uses an iterative technique to solve for the velocity and viscosity fields alternately and separately. At each iteration the viscosity and its gradient are assumed given, i.e., $\eta(\dot{\gamma})$ becomes $\eta(y)$. *Equation 4* is discretized on a grid where each grid point corresponds to a given streamfunction value ψ_i. The grid point positions are initially unknown and must be solved for (iteratively) as part of the

solution algorithm. *Figure 1* shows the geometry schematically for a two component flow and a small sample set of grid points. The set of streamlines is specified by fixing the values of ψ_i. The ψ_i are chosen so that each unknown interface corresponds to one of the given streamfunction values. When all the streamline positions are found (as described later) the interfaces will be known as well, but at each iteration they are assumed given at the latest guesses. Thus, within the iteration at the point of solving *Eq 4* everything is "known" except $v(y)$ and dp/dx.

Each derivative in the differential equation may be approximated by central differences on the nonuniform grid:

$$\left.\frac{dv}{dy}\right|_{y_i} \approx \frac{(v_{i+1}-v_i)(y_i-y_{i-1})^2 + (v_i-v_{i-1})(y_{i+1}-y_i)^2}{(y_{i+1}-y_i)(y_{i+1}-y_{i-1})(y_i-y_{i-1})}. \quad (8)$$

$$\left.\frac{d^2v}{dy^2}\right|_{y_i} \approx 2\,\frac{(v_{i+1}-v_i)(y_i-y_{i-1}) - (v_i-v_{i-1})(y_{i+1}-y_i)}{(y_{i+1}-y_i)(y_{i+1}-y_{i-1})(y_i-y_{i-1})}. \quad (9)$$

$$\left.\frac{d\eta}{dy}\right|_{y_i} \approx \frac{(\eta_{i+1}-\eta_i)(y_i-y_{i-1})^2 + (\eta_i-\eta_{i-1})(y_{i+1}-y_i)^2}{(y_{i+1}-y_i)(y_{i+1}-y_{i-1})(y_i-y_{i-1})}. \quad (10)$$

Equations 8 and *9* may be derived by fitting a parabola through the three points (y_{i-1}, v_{i-1}), (y_i, v_i), and (y_{i+1}, v_{i+1}) and then taking derivatives of the parabola. Equivalently, the equations may be derived in the classical way from second order Taylor series approximations for v_{i+1} and v_{i-1} based at y_i. Combining the two series to eliminate the second derivative terms gives *Eq 8*. Eliminating the first derivatives yields *Eq 9*. *Equation 10* is just *Eq 8* with "v" replaced by "η".

Substituting the finite difference formulas (*Eqs 8* and *9*) into *Eq 4* gives the equivalent finite difference equation:

$$[\eta_i b_i - d_i]v_{i-1} - [\eta_i a_i + \eta_i b_i + c_i - d_i]v_i + [\eta_i a_i + c_i]v_{i+1} = \frac{dp}{dx}; \qquad i = 0 \cdots N. \quad (11)$$

The coefficients are

$$a_i = \frac{2(y_i - y_{i-1})}{(y_{i+1}-y_i)(y_{i+1}-y_{i-1})(y_i-y_{i-1})},$$

$$b_i = \frac{2(y_{i+1} - y_i)}{(y_{i+1}-y_i)(y_{i+1}-y_{i-1})(y_i-y_{i-1})},$$

$$c_i = \left(\left.\frac{d\eta}{dy}\right|_{y_i}\right) \cdot \left(\frac{(y_i-y_{i-1})^2}{(y_{i+1}-y_i)(y_{i+1}-y_{i-1})(y_i-y_{i-1})}\right), \quad (12)$$

and

$$d_i = \left(\left.\frac{d\eta}{dy}\right|_{y_i}\right) \cdot \left(\frac{(y_{i+1}-y_i)^2}{(y_{i+1}-y_i)(y_{i+1}-y_{i-1})(y_i-y_{i-1})}\right).$$

Each viscosity, η_i, is assumed given. In fact, the viscosity on the grid points may be evaluated by using the previously calculated velocity in a central difference (*Eq 8*) for the shear rate, $\dot{\gamma}(y) = dv/dy$, and substituting into *Eq 5*, *6*, or *7* to yield $\eta(y)$. The derivatives $d\eta/dy$ may be calculated from these known viscosities using *Eq 10*. Note that for Newtonian flow $d\eta/dy = c_i = d_i = 0$. Also, for a uniform grid, $a_i = b_i$ and $c_i = d_i$.

On outer boundaries, i.e. the outer wall or the inner side of a material interface a central difference can no longer be used. The appropriate second-order difference formula for the velocity gradient comes from a parabola fit through the three points (y_i, v_i), (y_{i-1}, v_{i-1}), (y_{i-2}, v_{i-2}). The resulting formula for dv/dy follows.

$$\left.\frac{dv}{dy}\right|_{y_i} = \frac{(v_i - v_{i-1})(y_{i-1}-y_{i-2})(2y_i - y_{i-1} - y_{i-2})}{(y_i-y_{i-1})(y_i-y_{i-2})(y_{i-1}-y_{i-2})} - \frac{(v_{i-1}-v_{i-2})(y_i-y_{i-1})^2}{(y_i-y_{i-1})(y_i-y_{i-2})(y_{i-1}-y_{i-2})}. \quad (13)$$

On inner boundaries replace "$i - 1$" by "$i + 1$" and "$i - 2$" by "$i + 2$" in the above equation.

These boundary finite difference approximations are needed not only to evaluate the shear rate and viscosity, but to satisfy the boundary condition at interfaces between neighboring fluids, *A* and *B*. The shear stress must be continuous across the interface (in the absence of

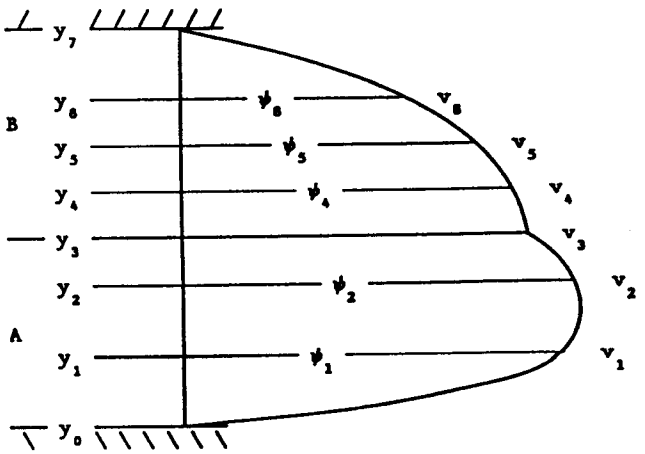

Fig. 1. Small sample streamlined finite difference grid illustrating the key variables and the geometry of the flow. M = 2; N = 7.

surface tension gradients).

$$\tau_{xy,A} = \tau_{xy,B}. \tag{14}$$

$$\frac{\eta_A}{\eta_B}\frac{dv_A}{dy} - \frac{dv_B}{dy} = 0. \tag{15}$$

Or, in finite difference form, taking phase A to be the inner phase,

$$\left[\frac{\eta_{A,i}}{\eta_{B,i}}\beta_{A,i}\right]v_{i-2} - \left[\frac{\eta_{A,i}}{\eta_{B,i}}(\alpha_{A,i} + \beta_{A,i})\right]v_{i-1} + \left[\frac{\eta_{A,i}}{\eta_{B,i}}\alpha_{A,i} - \alpha_{B,i}\right]v_i + [\alpha_{B,i} + \beta_{B,i}]\,v_{i+1} - [\beta_{B,i}]v_{i+2} = 0; \quad i = i_k; \quad k = 1 \cdots M-1. \tag{16}$$

with

$$\alpha_{A,i} = \frac{(y_{i-1} - y_{i-2})(2y_i - y_{i-1} - y_{i-2})}{(y_i - y_{i-1})(y_i - y_{i-2})(y_{i-1} - y_{i-2})}, \quad \text{and}$$
$$\beta_{A,i} = \frac{(y_i - y_{i-1})^2}{(y_i - y_{i-1})(y_i - y_{i-2})(y_{i-1} - y_{i-2})}. \tag{17}$$

Again, replace "$i - 1$" by "$i + 1$" and "$i - 2$" by "$i + 2$" to get the formulas for $\alpha_{B,i}$ and $\beta_{B,i}$.

The velocity field must also be continuous at the fluid boundary. This is handled implicitly by using only one value of v_i at each interface.

So far we have left implicit the nondimensionalization factors for the sequence of equations presented. In fact, all of the above equations keep the same form with dimensional or nondimensional variables. For numerical work it is helpful to nondimensionalize all variables to make them of the same order. Three characteristic values are sufficient to nondimensionalize all the variables used here: a characteristic length, $\bar{x}$, a characteristic velocity, $\bar{v}$, and a characteristic viscosity, $\bar{\eta}$. These are arbitrary, but the authors choose the gap width of the slit or annulus, the average velocity, and the viscosity of the most viscous fluid evaluated at the dimensionless shear rate, $\bar{v}/\bar{x}$.

SOLUTION METHOD

The equations as formulated above assume that the pressure gradient dp/dx is given and the velocity field is unknown. In the more common problem, the one to be solved here, the flow rate within each layer is given and the pressure gradient is unknown. The volume flow rate is an integral of the velocity field (the subscript 0 denotes the inner wall, N the outer).

$$Q = \int_{y_0}^{y_N} v(y)dy. \tag{18}$$

This equation could be added to the system of finite difference equations by making a numerical approximation to the integral (Simpson's rule, say) and moving dp/dx to the left side of the equations as an additional unknown. However, both the equation of motion and the boundary conditions are linear in v (if $\eta(y)$ is assumed given), so it is possible to take the pressure gradient as given at some nonzero level, calculate the corresponding velocity field, integrate for a calculated flow rate, and finally scale the velocity field linearly to achieve the desired flow rate. The pressure gradient will also be scaled by the same factor.

This approach saves the expense of adding an additional equation to the system (one which depends on all the variables). In addition, this idea of calculating the flow rate after solving the system and then making appropriate corrections may be extended as a method for moving the streamlines (including the interfaces) to their correct positions. If ψ_i is specified for a set of streamlines then *Eq 18* becomes an implicit equation for y_i.

$$\psi_i = \frac{1}{Q}\int_{y_0}^{y_i} v(y)dy; \qquad i = 0 \cdots N. \tag{19}$$

A rough algorithm based on the above approach is:

repeat
- solve for the velocity field (*Motion*)
- scale the velocity field for the desired total flow rate (*Continuity*)
- scale the pressure gradient similary (*Motion*)
- calculate the viscosity field (*Constitutive*)
- move the streamlines for correct flow rates between streamlines (*Continuity*)

until converged.

The above algorithm, as denoted to its right, effectively separates the equation of motion (including boundary conditions), the constitutive equation, and the continuity equation in an iterative procedure. The iteration is purely mechanical, not based on an actual time evolution; only the converged steady state solution has physical meaning. *Figure 2* presents details of the algorithm in flow chart form.

The primary step within each iteration is solving the system of difference equations (*Eqs 11* and *16*). This system is tridiagonal within each layer, but the band width undesirably increases to five for each interface grid point. A preliminary double Gauss elimination step at each boundary reduces the entire matrix to a tridiagonal one. This is illustrated schematically below:

```
X X X        X X X
↓
X X X X X →  X X X
      ↑
  X X X      X X X
```
(20)

Taking this step allows the system to be solved

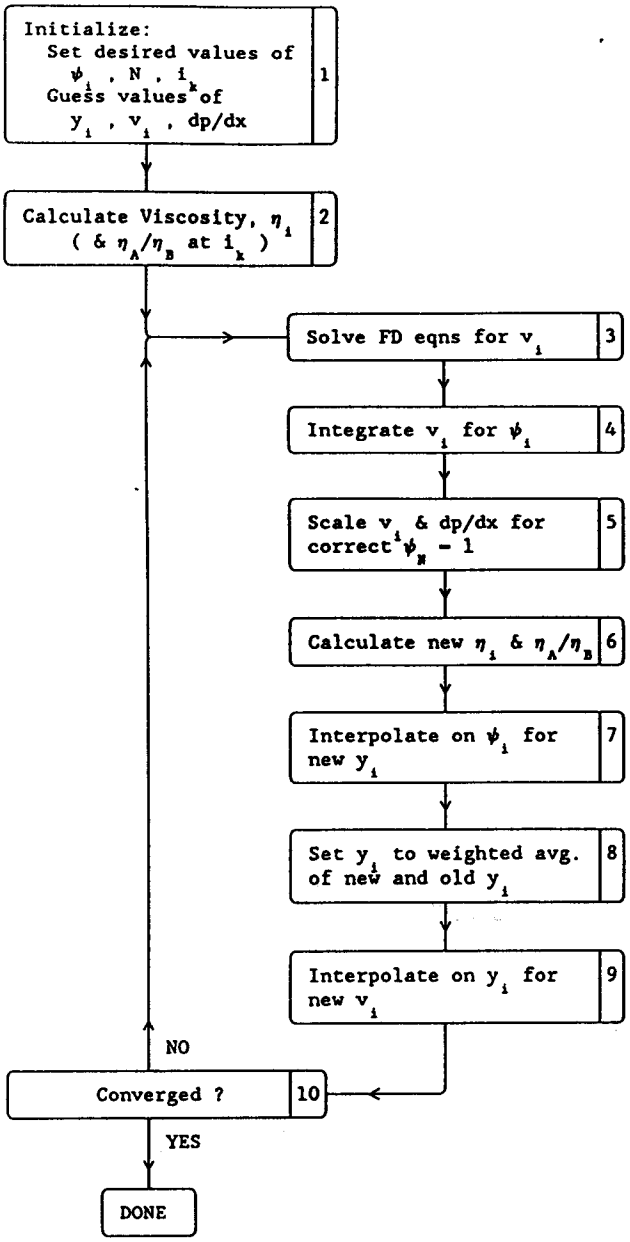

Fig. 2. Schematic flow chart of the streamlined finite difference solution algorithm.

efficiently with the well-known Thomas algorithm, e.g. (14), which is appropriate for diagonally dominant (in this case moderate viscosity gradient) tridiagonal systems.

The main advantage of the algorithm is that it converges on the needed values of y_i, v_i, and η_i simultaneously. The algorithm is fairly stable with respect to a poor guess for the initial velocity field. (The authors start with the profile for a single layer Newtonian flow). What is more important is to choose a set of streamfunction values, ψ_i, such that there is a fair number of streamlines (at least 10; even more for steep gradient areas) in every layer and such that streamline spacing ($y_i - y_{i-1}$) is reasonably uniform within each layer (to reduce inaccuracy in the finite difference approximations). Because the streamlines move at every iteration, a layer initially assigned ten streamlines will retain ten streamlines. The streamlines will automatically move where they are needed.

As it proceeds, the algorithm tends to oscillate in its guess for y_i at the interfaces, so some damping is actually put into the update for y_i (step 8 of *Fig. 2*). A simple underrelaxation is sufficient:

$$y_i = \omega y_{i,\text{old}} + (1 - \omega) y_{i,\text{new}}; \qquad 0 \le \omega \le 1 \quad (21)$$

The variable $y_{i,\text{new}}$ is the value of y_i that would be obtained directly from the interpolation, with no relaxation. Note that the smoothing step preserves the ordering of the y_i, $y_i < y_{i+1}$. A value of ω too high will result in overshooting of the iterative step; a value too low will mean no convergence. The algorithm therefore starts at $\omega = 0.5$ and then adjusts ω up or down (within limits) depending on whether convergence seems to be decelerating or accelerating. "Convergence" in the algorithm means that v_i, y_i, and dp/dx have all settled to stable values.

RESULTS AND DISCUSSION

When reliable experimental data are available, simulations may be done for realistic fluid models. Soskey (20) extensively characterized samples of LDPE and PS. *Figure 3* presents the power law, Carreau, and Wagner viscosity functions fit to his experimental data. The actual material parameters are available in (20). *Figure 4* presents a two-layer sheath/core pipe flow of these two materials modeled with truncated power laws, with Carreau models, and with viscoelastic models for both fluids. *Table 1* presents corresponding values of interface position, velocity, and viscosity ratio together with the pressure gradient for each simulation. The difference between fluid models is apparent. The power law gives a flatter velocity profile. The Carreau model smooths this out somewhat,

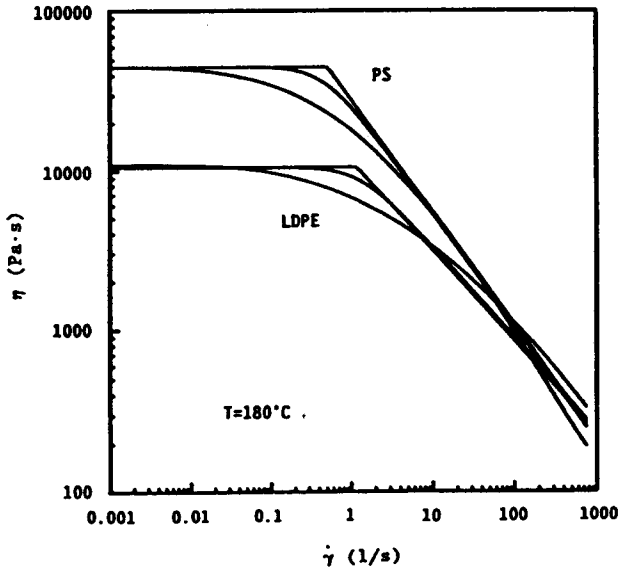

Fig. 3. Viscosities of LDPE and PS at 180°C (Soskey, 1984) comparing truncated power law, Carreau, and Wagner models.

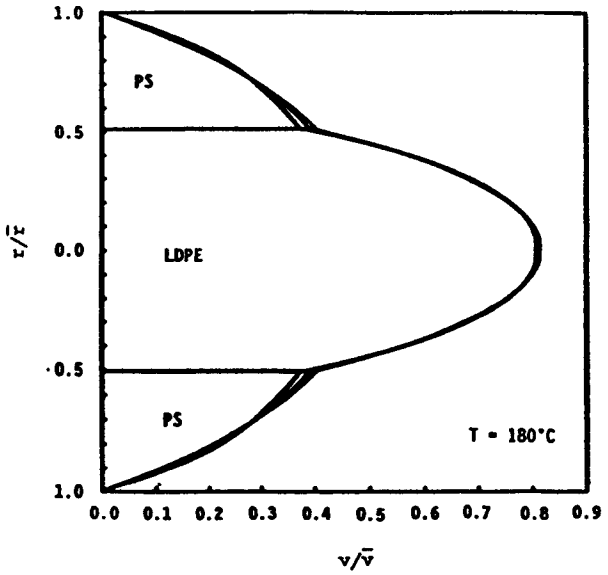

Fig. 4. Velocity profiles for flow of LDPE and PS at 180°C, comparing power law(PL), Carreau(C), and Wagner(W) model results.
$Q_{LDPE}/Q_{PS} = 1$; $\bar{r} = 10$ mm; $\bar{v} = 10$ mm/s.

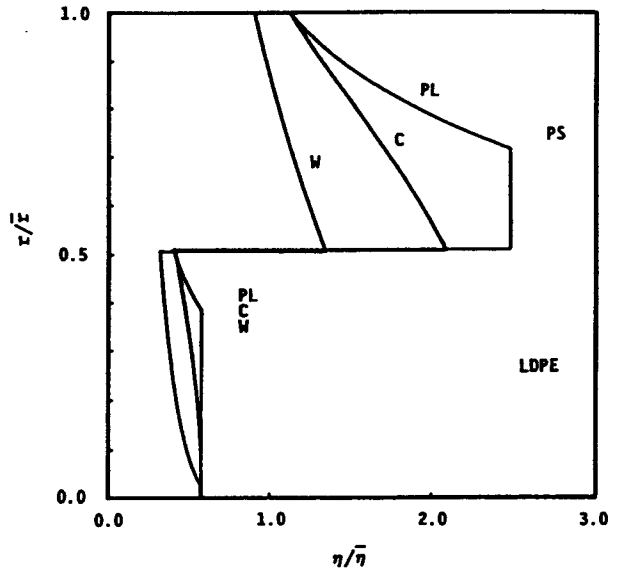

Fig. 5. Viscosity profiles for the flow of Fig. 4. $\bar{\eta} = 18025$ Pa·s.

Table 1. Results Corresponding to the Flow of *Fig. 4.*

	Interface			Pressure Gradient
	$r/\bar{r}$	$v/\bar{v}$	η_{LDPE}/η_{PS}	$(dp/dx)/(\bar{\eta}\bar{v}/\bar{r})$
Power Law	0.511	0.371	0.161	−3.589
Carreau	0.509	0.389	0.197	−3.190
Wagner	0.507	0.402	0.236	−2.319

$\bar{r} = 10$ mm; $\bar{v} = 10$ mm/s; $\bar{\eta} = 18025$ Pa·s

and the Wagner model, which models the viscosity at intermediate shear rates more closely, rounds the profile even more. This rounding is even more pronounced when the interface viscosity ratio is higher.

Figure 6 shows the viscosity profiles corresponding to *Fig. 5*. Here the disparity between fluid models is clear, partly because the flow was chosen so that most of the field fell in intermediate shear rate ranges where the constitutive models differ most. Truncating the power law prevents what would have been a very high viscosity ratio, but the ratio is still too high (or its reciprocal too low). *Table 1* also shows that the pressure gradient can be affected by the choice of constitutive model, something which is generally not true for single layer flows. In comparison, the velocity and position of the interface are relatively insensitive to the choice of viscosity model.

For viscoelastic fluids a first normal stress difference is observed even in simple shear flow. With the Wagner model the first normal stress coefficient can be calculated via an equation similar to *Eq 7:*

$$\Psi_1(\dot{\gamma}) = \sum_{i=1}^{m} \sum_{j=1}^{2} \frac{2f_j g_i \lambda_i^2}{(1 + n_j \lambda_i |\dot{\gamma}|)^3}. \qquad (22)$$

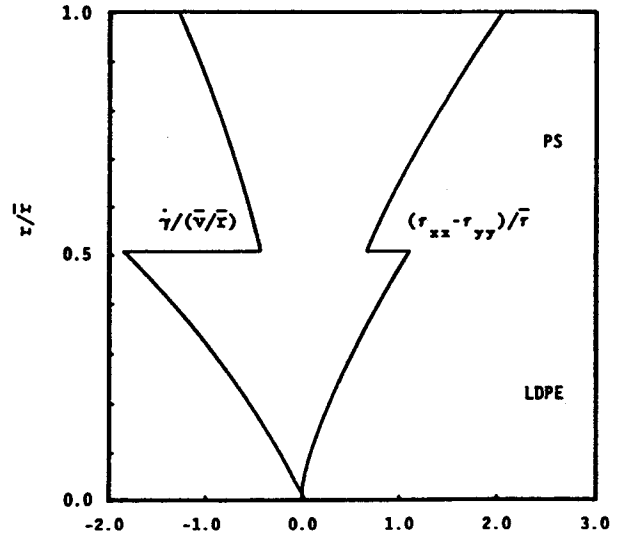

Fig. 6. First normal stress difference, $\tau_{xx} - \tau_{yy}$, and shear rate profiles for the flow of Fig. 4.
$\bar{\tau} = 18025$ Pa; $\bar{v}/\bar{r} = 1.0$

Figure 6 shows the first normal stress difference, $\sigma_{xx} - \sigma_{yy}$, calculated with this equation for the flow of *Fig. 4*. Also shown is the shear rate, $\dot{\gamma}$. Jumps in the normal stress difference as observed here can cause instabilities in the flow, depending on the geometry (21). The reason is that the normal stress perpendicular to the interface, σ_{yy}, must be continuous, so the jump is actually a jump in the tension on the interface, σ_{xx}. If this effect increases with curvature then the flow is unstable. The method of this paper could become a tool to predict interface instabilities based on empirical observations of conditions when instabilities occur.

In coextrusion die design a common goal is to *minimize* viscosity and normal stress jumps across layers in order to avoid instabilities. For this purpose the power law clearly gives un-

realistic results. The calculated viscosity jump is either too huge to be realistic or is artificial because of truncation.

As an example of how the method could be applied to a multilayer flow more typical of commercial applications, *Figure 7* presents a seven layer planar flow in which thick polymer layers partially alternate with thin tie layers. *Figure 8* presents the viscosity profile corresponding to *Fig. 7*. The tie layers are Newtonian; the other layers are various Carreau fluids. The flow shown is purely arbitrary, but similar, more realistic flows could be easily modeled, given accurate material parameters.

Multi-layer flows are not limited to Poiseuille flows. *Figure 9* presents a two-layer wire coating flow which is both drag and pressure driven.

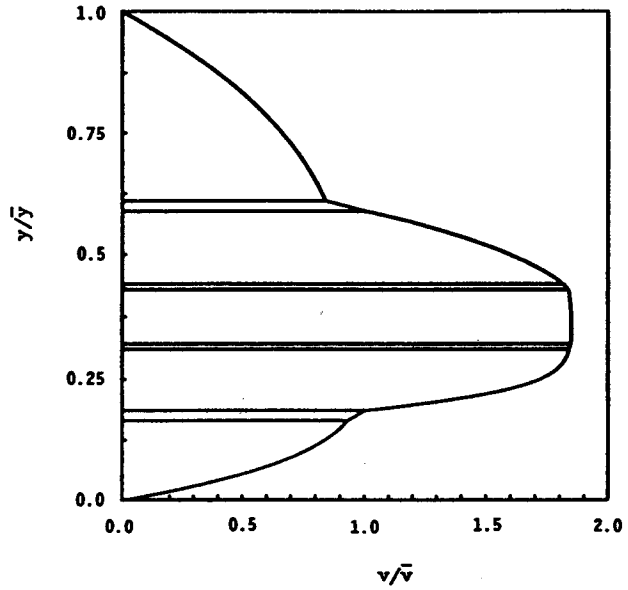

Fig. 7. Velocity profile for a hypothetical nine layer flow of various Carreau fluids. Relatively thick low viscosity tie layers separate polymer layers, illustrating the power of the method for practical use.

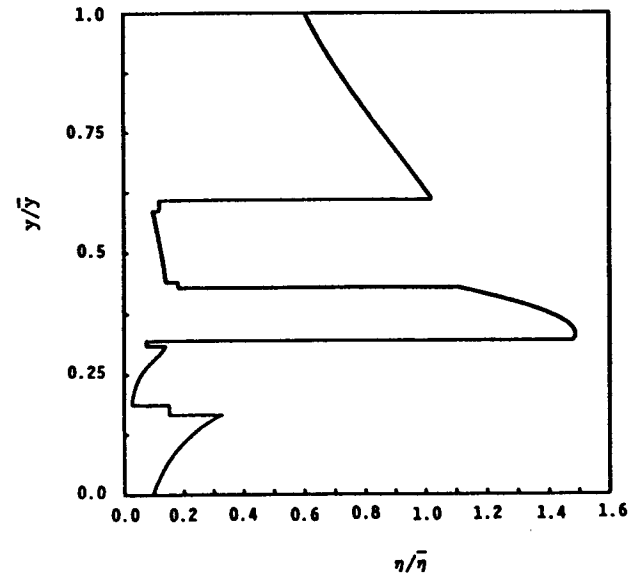

Fig. 8. Viscosity profile for the flow of Fig. 7.

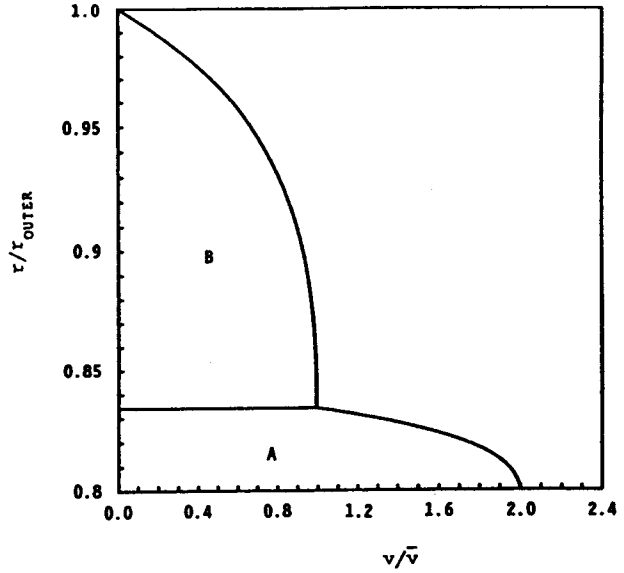

Fig. 9. Velocity profile for a wire coating flow of two power law fluids.
A: $\dot{\gamma}^0 = 1$; $\eta^0 = 1$; $n = 0.4$; $\eta_0 = 10^5$; $Q_A/Q = 0.3$
B: $\dot{\gamma}^0 = 1$; $\eta^0 = 10$; $n = 0.3$; $\eta_0 = 10^5$; $Q_B/Q = 0.07$

This flow is for two simple power law fluids. Normally the power law *must* be truncated in numerical work to avoid machine overflow. However, the wire coating flow of *Fig. 9* has no zero shear rate point, so the truncation, if high enough, becomes irrelevant, and a comparison with semi-analytical results becomes possible. In fact *Fig. 9* plots both the numerically calculated profile and the semi-analytical profile calculated by the shooting procedure described in the *Introduction*. The two are virtually indistinguishable. The numerical procedure gives a slightly lower interface velocity, but pressure gradients and interface positions are identical for the two methods.

CONCLUSIONS

The numerical method we have described efficiently solves fully developed multilayer non-Newtonian shear flows for fluids with realistic shear viscosity constitutive equations. For the power law results can be favorably checked against an analytical solution. However, the power law, though sufficient for predicting pressure gradients and interface positions, gives unrealistically flat velocity profiles even when numerically truncated at finite viscosity. For the die designer's common task of trying to match viscosities at interfaces (through temperature control) the power law is clearly useless.

This step of viscosity matching is most important in areas of high stress. Near the center of the flow viscosity jumps have smaller effects on the velocity profile and shear rate (e.g., *Fig. 5*). In viscoelastic polymers shear rate jumps can cause corresponding jumps in the first normal stress difference across interfaces. For dissimilar materials this normal stress difference jump can be extreme and is the cause of insta-

bilities in the flow. The present method could become a numerical tool for studying the onset of instability for fluids with complicated rheological behavior.

The ability to specify the viscosity numerically, separately from the equation of motion, makes the fully developed streamlined finite difference method an appropriate building block for studying nearly fully developed multilayer flows. These include lubrication flows, developing nonisothermal flows, and narrow channel distribution flows. Work in these areas is in progress.

ACKNOWLEDGMENT

The authors gratefully acknowledge the support of GE Plastics, Pittsfield, MA. M. E. Nordberg III acknowledges additional support as a Graduate Fellow of the National Science Foundation.

APPENDIX; AXISYMMETRIC FLOW FINITE DIFFERENCE EQUATIONS

This section parallels the derivation for planar flow in the body. Equation numbers correspond to those in the earlier section.

For axisymmetric flow the equation of motion is

$$\frac{1}{r}\frac{d}{dr}(r\tau_{rz}) = \frac{dp}{dz}. \tag{A.1}$$

The shear stress is again that of a purely viscous fluid:

$$\tau_{rz} = \eta(\dot{\gamma})\frac{dv}{dr}. \tag{A.2}$$

Substituting gives

$$\frac{1}{r}\frac{d}{dr}\left(r\eta(\dot{\gamma})\frac{dv}{dr}\right) = \frac{dp}{dz}. \tag{A.3}$$

Expanding the derivatives gives

$$\frac{\eta(\dot{\gamma})}{r}\frac{dv}{dr} + \eta(\dot{\gamma})\frac{d^2v}{dr^2} + \frac{dv}{dr}\frac{d\eta}{dr} = \frac{dp}{dz}. \tag{A.4}$$

With central differences for the derivatives the above equation can be expressed in difference form:

$$[\eta_i b_i - d_i]v_{i-1} - [\eta_i a_i + \eta_i b_i + c_i - d_i]v_i + [\eta_i a_i + c_i]v_{i+1} = \frac{dp}{dx}; \qquad i = 0 \cdots N. \tag{A.11}$$

The coefficients are now

$$a_i = \frac{2(r_i - r_{i-1})}{(r_{i+1} - r_i)(r_{i+1} - r_{i-1})(r_i - r_{i-1})},$$

$$b_i = \frac{2(r_{i+1} - r_i)}{(r_{i+1} - r_i)(r_{i+1} - r_{i-1})(r_i - r_{i-1})},$$

$$c_i = \left(\left.\frac{d\eta}{dr}\right|_{r_i} + \frac{\eta_i}{r_i}\right) \cdot \left(\frac{(r_i - r_{i-1})^2}{(r_{i+1} - r_i)(r_{i+1} - r_{i-1})(r_i - r_{i-1})}\right), \tag{A.12}$$

and

$$d_i = \left(\left.\frac{d\eta}{dr}\right|_{r_i} + \frac{\eta_i}{r_i}\right) \cdot \left(\frac{(r_{i+1} - r_i)^2}{(r_{i+1} - r_i)(r_{i+1} - r_{i-1})(r_i - r_{i-1})}\right).$$

All other equations in the text, including the finite difference formulas (*Eqs 8* to *10*) and the relations describing interface boundaries (*Eqs 14* to *17*) may be used as is except that "y" becomes "r" and "x" becomes "z". The only other equation that changes form is the flow rate calculation within the solution algorithm. It is now

$$\psi_i = \frac{1}{Q}\int_{r_0}^{r_i} rv(r)dr; \qquad i = 0 \cdots N. \tag{A.19}$$

NOMENCLATURE

a, b, c, d	=	Finite difference equation coefficients (motion).
f_j	=	Strain functional parameters.
g_i	=	Spectrum of viscoelastic moduli.
i	=	(Subscript) streamline number.
k	=	(Subscript) interface number.
m	=	Number of time constants in viscoelastic spectrum.
M	=	Number of layers.
n	=	Power law index.
n_j	=	Strain functional parameters.
N	=	Total number of streamlines.
P	=	Pressure.
Q	=	Total volume flow rate.
r	=	Coordinate perpendicular to annular flow.
v	=	Velocity.
x	=	Coordinate parallel to planar flow.
y	=	Coordinate perpendicular to planar flow.
z	=	Coordinate parallel to annular flow.
α_A, α_B β_A, β_B	=	Finite difference equation coefficients (B.C.).
$\dot{\gamma}$	=	Shear rate.
$\dot{\gamma}^o$	=	Power law reference shear rate.
η	=	Viscosity.
η_o	=	Zero shear rate viscosity.
η_∞	=	Infinite shear rate viscosity.
η^o	=	Power law reference viscosity.
τ_{xy} or τ_{rz}	=	Shear stress.
$\sigma_{xx} - \sigma_{yy}$	=	First normal stress difference.
ψ_i	=	Normalized streamfunction value for streamline i.
Ψ_1	=	First normal stress coefficient, $(\sigma_{xx} - \sigma_{yy})/\dot{\gamma}$.

ω = Weighting coefficient for damped iteration.

REFERENCES

1. W. J. Schrenk and T. Alfrey, Jr., in *Polymer Blends and Composites*, J. A. Mason and L. H. Sperling, Eds., Plenum, New York, (1976).
2. A. Ya. Malkin, M. L. Friedman, K. D. Vachaghin, and G. V. Vinogradov, *J. Appl. Polym. Sci.*, 19, 375 (1975).
3. C. D. Han and H. B. Chin, *Polym. Eng. Sci.*, 19, 1156 (1979).
4. M. E. Nordberg, III, Ph.D. Thesis, University of Massachusetts, (in progress).
5. S. Basu, *Polym. Eng. Sci.*, 21, 1128 (1981).
6. E. Uhland, *Polym. Eng. Sci.*, 17, 671 (1975).
7. N. Minagawa and J. L. White, *Polym. Eng. Sci.*, 15, 825 (1975).
8. A. Karagiannis, H. Mavridis, A. N. Hrymak, and J. Vlachopoulos, *SPE ANTEC Tech. Papers*, 33, 106 (1987).
9. W. J. Schrenk, N. L. Bradley, T. Alfrey, and H. Maack, *Polym. Eng. Sci.*, 18, 620 (1978).
10. E. Mitsoulis, *J. Rheology*, 30(S), S23 (1986).
11. G. Sornberger, B. Vergnes, and J. F. Agassant, *Polym. Eng. Sci.*, 26, 456 (1986).
12. C. D. Han and R. Shetty, *Polym. Eng. Sci.*, 16, 697 (1976).
13. C. D. Han, *Multiphase Flow in Polymer Processing*, Academic Press, New York, (1981).
14. R. L. Burden, J. D. Faires, and A. C. Reynolds, *Numerical Analysis, 2nd Ed.*, Prindle, Weber and Schmidt, Boston (1981).
15. H. Mevridis, A. N. Hrymak, J. Vlachopoulos, *AIChE J.*, 33(3), 410 (1987).
16. A. C. Papanastasiou, L. E. Scriven, and C. W. Macosko, *J. Non-Newt. Fluid Mech.*, 22, 271 (1987).
17. X.-L. Luo and R. I. Tanner, *J. Non-Newt. Fluid Mech.*, 21, 179 (1986).
18. X.-L. Luo and R. I. Tanner, *J. Non-Newt. Fluid Mech.*, 22, 61 (1986).
19. H. M. Laun, *Rheol. Acta*, 17, 1 (1978).
20. P. R. Soskey, Ph.D. Thesis, University of Massachusetts, (1984).
21. C. D. Han and R. Shetty, *Polym. Eng. Sci.*, 18, 180 (1978).